Int. J. Electrochem. Sci., 17 **(2022)** Article Number: 2212100, doi: 10.20964/2022.12.105

International Journal of
ELECTROCHEMICAL
SCIENCE
www.electrochemsci.org

An Electrochemical Sensor with Graphene–Graphene Oxide Nanocomposite and Ammonium Molybdate for Phosphate Determination

Yaw-Jen Chang[1,*], *Yi-Chien Chen*[1], *You-Chiuan Chien*[1,2]

[1] Department of Mechanical Engineering, Chung Yuan Christian University, Chung Li District, Taoyuan City, 32023, Taiwan
[2] Changhua Christian Hospital, Changhua City, Changhua County 500, Taiwan
[*]E-mail: justin@cycu.edu.tw

Received: 13 September 2022 / *Accepted:* 28 November 2022 / *Published:* 27 December 2022

This paper presents an electrochemical sensor for the quantitative determination of phosphate. The sensor's working electrode was modified with a layer of graphene–graphene oxide nanocomposite and ammonium molybdate. The reaction of phosphate and ammonium molybdate forms a phosphomolybdate complex on the electrode. Furthermore, the nanocomposite with a proper mixing ratio can immobilize the phosphomolybdate for cyclic voltammetry (CV) measurement since it possesses both the high conductivity of graphene and the polyfunctional groups of graphene oxide. The experimental results show that the absolute value of peak reduction current at -0.21 V increased with the increase of phosphate concentration and exhibited a linear relationship in the concentration range of 0.2–5 mM. This proposed sensor is suitable for detecting phosphate levels in the physiological and higher concentration ranges. Moreover, all possible interfering substances in both urethral calculus and human blood, except for copper ions, do not influence the detection of phosphate using this proposed sensor. Therefore, it can be used to detect the content of phosphate in urethral calculus or human blood.

Keywords: Phosphate, Graphene–Graphene Oxide Nanocomposite, Ammonium Molybdate, Cyclic Voltammetry

1. INTRODUCTION

Phosphate, derived from phosphoric acid, is an essential substance in the environmental and biological systems. In the environmental system, excessive phosphate induces the mass growth of microbes and the oxygen content in water is consumed rapidly, leading to the eutrophication phenomenon and the death of other organisms. On the other hand, the phosphate in the micro-system is an indispensable molecule for all living creatures, particularly in all mineral reactions of bones [1]. In the human body, phosphate is involved in the constitution of human body structure, such as bone and tooth composition, metabolic activation (glucose metabolism), energy transfer and storage, and acid-base balance in the body fluids [2-4]. In physics, phosphate mainly comes from food and is mostly a mixture of organic and inorganic phosphorus. In the small intestine, digested phosphorus undergoes hydrolysis to form inorganic phosphate, which is absorbed largely via paracellular phosphate transport [5]. To maintain constancy, the serum level of phosphorus in the human body remains in a stable range (2.5 – 4.5 mg/dL). However, in some extreme conditions, such as high phosphorus, food is ingested without sufficient water intake or excessive water loss, in which the kidneys fail to excrete excessive phosphorus from the body, inducing hyperphosphatemia (> 4.5 mg/dL) [6]. Hyperphosphatemia may cause an imbalance in calcium metabolism and even secondary hyperparathyroidism [7]. On the other hand, when the serum level of phosphate is lowered, hypophosphatemia (< 2.5 mg/dL) induces neurological abnormalities, such as paresthesia, thrill, hyperreflexia, ataxia, and even coma. Chronic hypophosphatemia also reduces the 2-3-diphosphoglycerate (2-3-DPG), which results in the shorter life span of erythrocytes, hemolysis, and osteomalacia, including ostealgia or pseudofracture in long-term change [8, 9].

Additionally, the phosphate concentration in the urinary system is tightly correlated with infectious urinary tract stones. Magnesium ammonium phosphate (MAP) is a common constituent of human urine. An unsaturated level of MAP in urine is not a physical burden on the human body. When the phosphate concentration in blood is beyond the clearance of kidney or bacteria overgrowth in the urinary system, phosphate concentration in urine may gradually reach saturation or over-saturation. Thus, the excess phosphorus ions induce the $MAP \cdot H_2O$ in urine to form $MAP \cdot 6H_2O$ micro-crystal. The $MAP \cdot 6H_2O$ micro-crystals will continue to be hydrolyzed, transformed, and crystallized with the other molecules in urine, gradually forming calculi in the kidneys [10, 11]. Urinary stone is a major medical problem in the urology departments of Taiwan hospitals, where the treatment strategy varies with the composition of urinary calculi of different patients. Once phosphate is found in the urinary stone composition, the clinical treatment protocol would be switched to controlling infections. Along with removing the urinary stone, the doctor needs to administer antibiotics to treat the patient’s urinary tract infection to overturn the sickness and further avoid recurrence [12, 13].

Therefore, phosphate detection is not only an important tool in environmental surveillance, but also a diagnostic tool to survey phosphate conditions in human physiology. In addition, clinical doctors may utilize it as a sentinel to detect urinary tract infections.

Various analytical approaches have been developed for phosphate determination, including colorimetry [14-17], chemiluminescence [18-20], and electrochemical analysis. Without using potentially toxic agents, electrochemical techniques can detect phosphate by amperometry [21-23] and cyclic voltammetry (CV) [24], among others. These techniques exhibit simplicity and offer a high degree of sensitivity based on the interaction of electrical energy and matter.

This study presents an electrochemical approach for the quantitative determination of phosphate contained in calcium phosphate. This approach aims to analyze the phosphate content in urinary stones. In this study, the electrode of the electrochemical sensor was modified with a nanocomposite layer, a mixture of graphene (G) and graphene oxide (GO). Graphene-based materials have been one of the most attractive and ideal materials in the development of electrochemical sensors [25-30]. Graphene is a one-atom-thick graphite. Its carbon atoms exist in sp^2 form, and three carbon atoms bond together to form a two-dimensional honeycomb structure. Graphene materials exhibit excellent properties, such as superior electron mobility, excellent electrical conductivity, and high surface area. Graphene oxide, on the other hand, is a highly oxidized derivative of graphene and has the same hexagonal lattice structure as graphene. The basal plane and edges of graphene oxide contain multiple functional groups, including carbonyl (C-O), hydroxyl (C-OH), epoxy (C=O), and carboxyl (COOH). Thus, graphene oxide has excellent adsorbability and catalytic capability, providing anchor points for the reactants due to its amphiphilic and functional properties. Since the two materials have the same physical properties, they were mixed in this study to simultaneously highlight the high conductivity of graphene and the polyfunctional groups of graphene oxide. Moreover, ammonium molybdate was utilized for phosphate determination. Ammonium molybdate is the most commonly used compound in measuring phosphate content by the colorimetric method based on the blue phosphomolybdate complex formed by the reaction of phosphate and ammonium molybdate [14, 16, 17, 31, 32]. Furthermore, graphene–graphene oxide nanocomposite was prepared to immobilize the phosphomolybdate, and cyclic voltammetry was employed for detection.

2. EXPERIMENTAL

2.1 Materials

The paper-based chip, with three screen-printed carbon electrodes (SPE), was purchased from Zensor R&D Corp. (Taiwan). Graphene (Powder, 8 nm flakes) was purchased from Graphene Supermarket (USA). The graphene oxide was synthesized from graphite powder using a modified Hammer’s method. The materials necessary for synthesizing the graphene oxide include graphite (purchased from SIGMA-Aldrich), H_2SO_4, Na_2SO_4, $KMnO_4$, H_2O_2, and dialysis membrane.

In this study, $(Ca(H_2PO_4)_2)\cdot H_2O$ (99% extra pure powder) purchased from Scharlau (Spanish) served as the analyte. Determining phosphate content in calcium phosphate is essential for analyzing the ingredient of urethral calculus. Moreover, ammonium molybdate (abbreviated as AMT) is a compound usually used as an analytical reagent to measure the amount of phosphates. Thus, AMT (chemical formula: $(NH_4)_6Mo_7O_{24}$, powder, > 98%) was used for surface modification of the SPE electrodes. For CV measurements, a 0.65 M sulfuric acid buffer solution was prepared.

2.2 Surface modification

An appropriate electrode surface that specifically reacts with phosphate is a prerequisite for reaching good selectivity in phosphate detection. AMT is known to react with phosphate and produce phosphomolybdate, allowing CV measurement to determine phosphate. Hence, a nanocomposite layer of graphene and graphene oxide was coated on the electrode of SPE to immobilize the AMT.

Graphene and graphene oxide were added to deionized (DI) water to prepare the G-GO aqueous solution with a weight percentage of 10%, which was stirred with an ultrasonic oscillator. Afterward, 5 μL of mixed G-GO aqueous solution was instilled onto the working electrode of SPE and dried in the oven at 37°C to complete the deposition of G-GO nanocomposite on the SPE. The current chip was marked as G-GO/SPE. Next, 1.2583 g of AMT was dissolved in 97.417 mL of DI water using the ultrasonic oscillator. Then, 10 μL of AMT aqueous solution was drop casted onto the G-GO nanocomposite layer on SPE and dried in a 37°C hot circulator oven. This chip is labeled AMT/G-GO/SPE.

2.3 CV experiment

In this study, the CV measurement method was employed to detect the phosphate concentration in calcium phosphate. Since calcium phosphate is insoluble in water, an acid buffer solution was necessary. In addition to dissolving calcium phosphate, the acid buffer solution also participates in the reaction of phosphomolybdate. The reaction of phosphate ions in the presence of molybdate in acidic media [23, 33] is as follows:

$$7H_3PO_4 + 12Mo_7O_{24}^{6-} + 51H^+ \rightarrow 7[PMo_{12}O_{40}]^{3-} + 36H_2O$$

Therefore, the experimental steps are as follows. First, calcium phosphate was dissolved in a sulfuric acid buffer solution. A drop of 200 μL test solution was sucked and dripped to cover the three electrodes of AMT/G-GO/SPE. After the reaction of AMT with phosphate for 240 s, a cyclic voltammetry measurement was performed. The cyclic voltammetry was carried out with a sweep potential between -0.6 to 0.8 V at a scan rate of 50 $\mathrm{mVs^{-1}}$. For each concentration, three AMT/G-GO/SPE sensors were prepared for repetitious experiments. The redox reaction equation of cyclic voltammetry is as follows:

$$[PMo_{12}O_{40}]^{3-} + ne^- + nH^+ \leftrightarrow [H_nPMo_n^5/Mo_{12-n}^6O_{40}]^{3-}$$

3. RESULTS AND DISCUSSION

3.1 Result of surface modification

The variation of the chip surface before and after the electrochemical experiment on phosphate was observed through field emission scanning electron microscopy (FE-SEM). Only the G-GO nanocomposite was coated on the SPE before the electrochemical experiment. In the SEM image at 5000-magnification, as shown in Figure 1(a-1), the G-GO nanocomposite displayed a wrinkled structure with plenty of white corrugations, which resulted from the slight changes in height during the stacking of flaky graphene and graphene oxide. This result is consistent with the typical morphology of graphene-based materials, showing wrinkled and folded textures [34-37]. Figure 1(a-2) presents the elemental analysis of this sample using energy-dispersive X-ray spectroscopy (EDS). The result of EDS demonstrated that only carbon and oxygen were detected.

After the ionic reaction of molybdophosphoric acid and redox reaction of cyclic voltammetry, the phosphomolybdate should be generated on the electrode surface according to the above reaction formulas. As shown in Figure 1(b-1), there were particle objects on the electrode surface, apart from the original corrugations. In order to confirm that these particles were not atmospheric aerosol particulates, EDS was used again for the elemental analysis of this sample. As shown in Figure 1(b-2), the EDS result indicated that this sample contained phosphorus (P) and molybdenum (Mo) in addition to carbon and oxygen. The sulfur (S) element came from the sulfuric acid buffer solution. This result proves that the particle crystal was not a particulate but a phosphomolybdate crystal. In other words, the G-GO nanocomposite can effectively immobilize AMT so that phosphomolybdate crystals can be generated after the electrochemical experiment.

Before the electrochemical experiment on phosphate

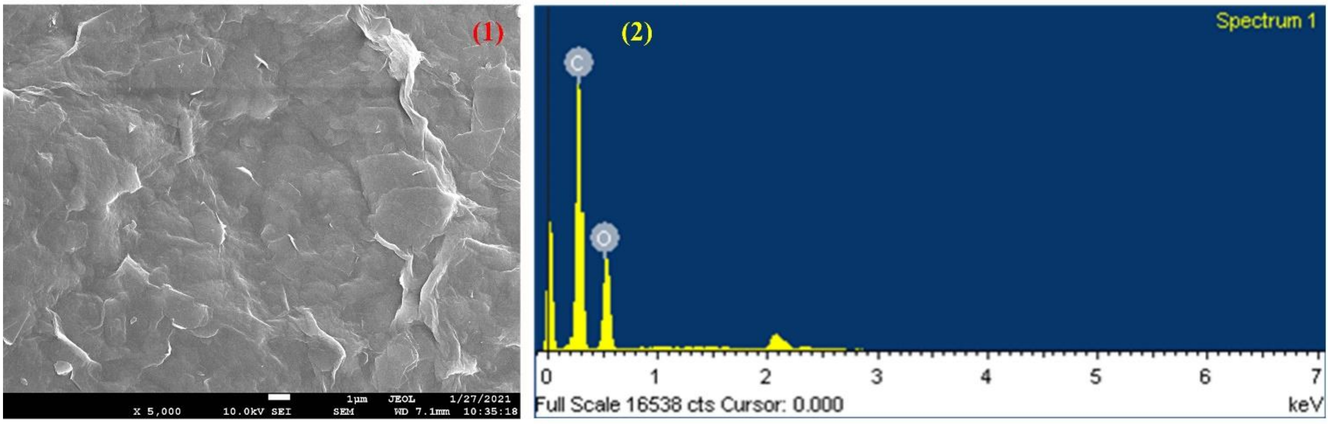

(a)

After the electrochemical experiment on phosphate

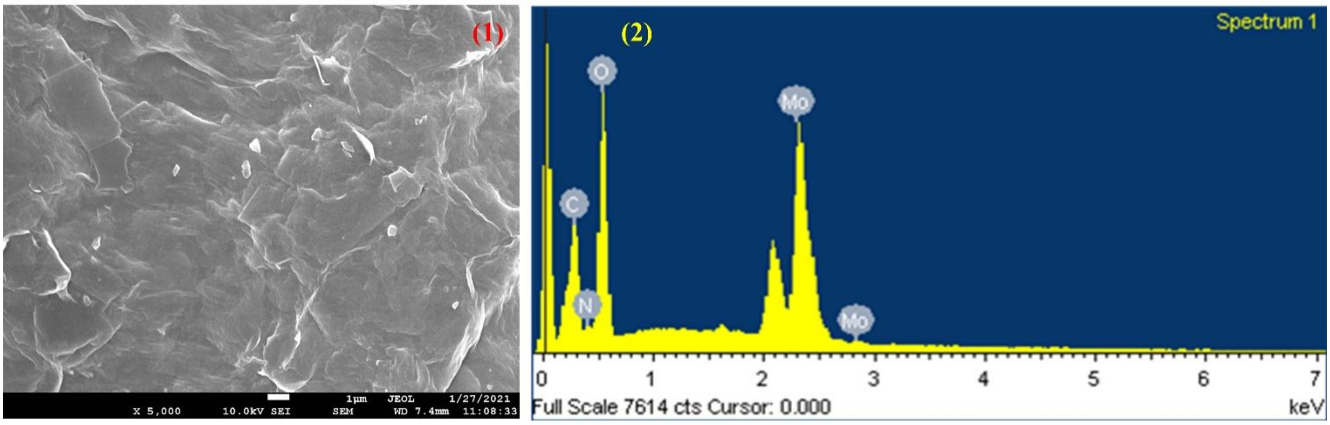

(b)

Figure 1. SEM and EDS of electrode surface: (a) Before the electrochemical experiment. (b) After the electrochemical experiment on phosphate.

3.2 Comparison of different G-GO mixing ratios

To validate whether G-GO nanocomposite possesses both high conductivity and sufficient functional groups, the authors of this study designed different mixing ratios of graphene and graphene oxide for comparison—that is, the ratios of graphene to graphene oxide were 1:2, 1:3, and 1:4, respectively. Additionally, the G-GO mixture accounted for 10% wt of the solution. For instance, in the 1:4 G-GO mixed solution, 0.2 g graphene and 0.8 g graphene oxide were added into 9 mL DI water and mixed thoroughly. Similarly, the G-GO solution with other mixing ratios can be prepared by changing the grams of graphene and graphene oxide.

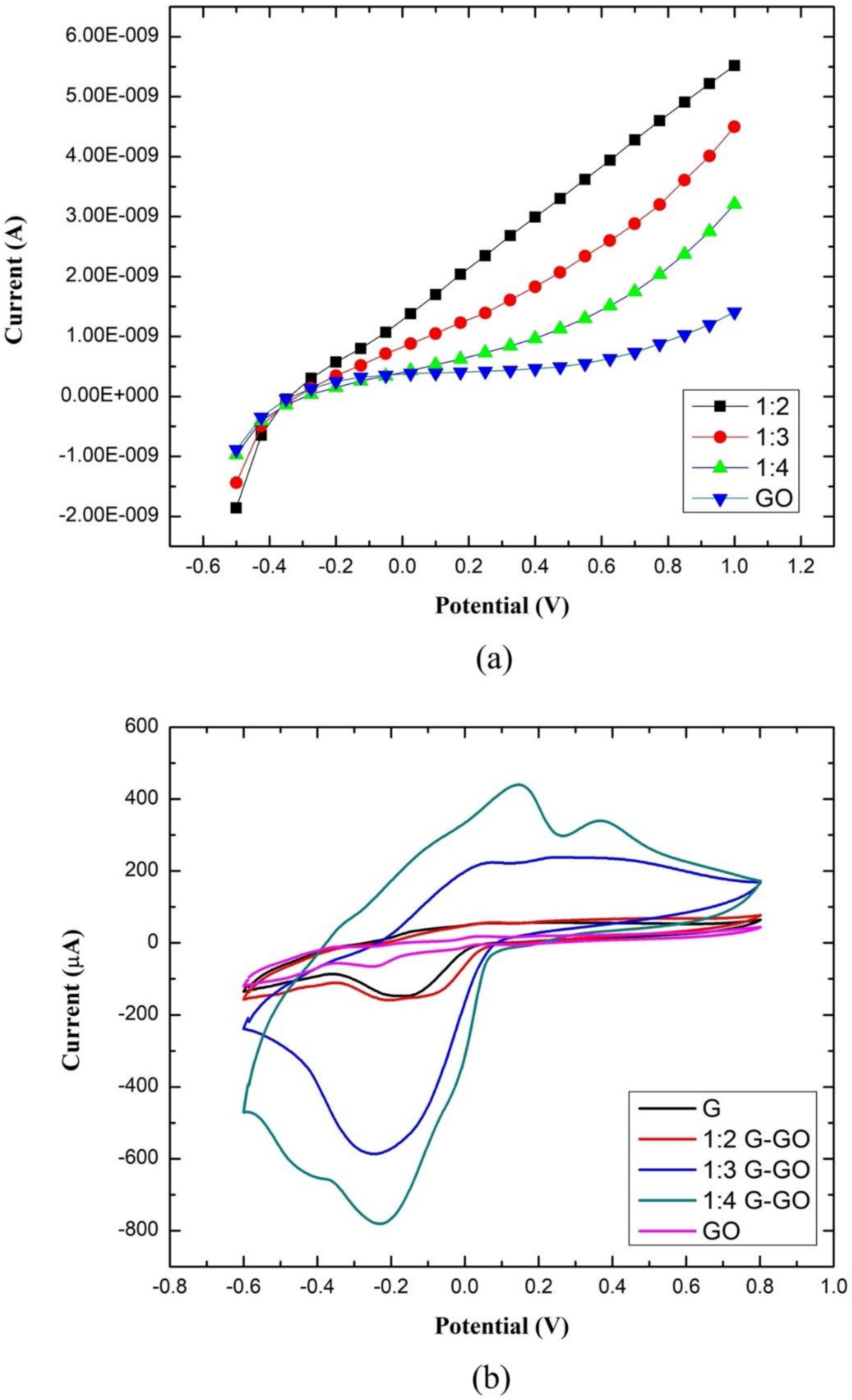

(a)

(b)

Figure 2. Comparison of different G-GO nanocomposites: (a) The I-V curves of G-GO nanocomposites with different mixing ratios. (b) Cyclic voltammograms of different G-GO nanocomposites to measure 5 mM test solutions prepared by dissolving calcium phosphate.

Then, 5 μL of G-GO mixed solution was instilled onto the working electrode of SPE. The chip was baked in the oven at 37°C for 30 min. Afterward, 0.65 M of sulfuric acid buffer solution was employed as an electrolyte for the electrical measurement, which was conducted using a high-accuracy electric meter (Keithley 2614B) with a voltage ranging from -0.5 to 1.0 V. As shown in Figure 2(a), the experimental results revealed that, in different proportions of G-GO nanocomposites, the working electrode of SPE had a larger current-to-voltage (I-V) response as the content of graphene increased and the content of graphene oxide decreased. It is in line with common sense that graphene has excellent electrical conductivity, unlike graphene oxide. Moreover, the electrical conductivity of other graphene-based composites, such as graphene- and graphene oxide-doped micro-nanofibrillated cellulose (MFC/NFC), was reported to have similar results [38]. The MFC/GO composite showed bad electrical conductivity because GO is an insulator.

The next step was to test the properties of the functional groups of the G-GO nanocomposite to anchor the phosphomolybdate using a 5 mM test solution prepared by dissolving calcium phosphate. The experimental results, as shown in Figure 2(b), disclosed that the reaction current of the pure GO-modified chip was the smallest, given the poor conductivity of pure graphene oxide. When the mixing ratio was 1:4, the absolute value of the peak reduction current increased from 60.2 μA of pure GO modification to 780 μA. The electrochemical performance was enhanced by about 13 times. When the mixing ratio is 1:2, the content of graphene is higher than that of the mixing ratio 1:4; theoretically, the electrical conductivity of 1:2 G-GO should be better. However, lower GO content cannot provide adequate high specific surface areas and enough functional groups to anchor the phosphomolybdate, leading to lower peak oxidation current. Therefore, only a proper G-GO mixing ratio can achieve the goal of high conductivity and sufficient functional groups. The experimental result showed that 1:4 was the optimal ratio in this study, and the 1:4 G-GO mixed solution was adopted as the electrode modification material.

3.3 Comparison of different electrodes

Four kinds of modified working electrodes were used in this experiment to detect a 1 mM test solution of calcium phosphate by cyclic voltammetry to verify the importance of AMT for phosphate detection: (1) Bare SPE, (2) G-GO/SPE, (3) AMT/SPE, and (4) AMT/G-GO/SPE. The cyclic voltammograms were recorded for comparison, as shown in Figure 3. In the detection with Bare SPE and G-GO/SPE, phosphate was inactive to electrochemistry, and there was almost no redox reaction. Since phosphoric acid can buffer the pH value of a solution, it is often used as an experimental buffer solution. Without AMT, phosphate cannot undergo the ionic reaction to produce molybdophosphoric acid for the redox reaction. In this case, phosphate functioned as a buffer; hence, there was no redox reaction.

When AMT/SPE and AMT/G-GO/SPE were adopted for detecting phosphate, apparent CV peaks were observed. This phenomenon indicated that AMT and phosphate generated molybdophosphoric acid ions in acidic media, allowing the redox reaction to occur with electrons transfer in the electrochemical experiment. Therefore, AMT is essential for phosphate detection.

Moreover, AMT/G-GO/SPE had the largest peak current in the phosphate detection of these four modified electrodes. Except for the function of AMT to detect phosphate, the higher electrical conductivity of G-GO nanocomposite contributes to phosphate detection, resulting in the largest peak current.

There are various methods to detect phosphate. However, AMT is the most commonly used compound. For previous literatures on phosphate detection using AMT [23, 31, 33, 39, 40], their results suggested that AMT was essential for phosphate detection, although different materials were used for the surface modification of the electrode.

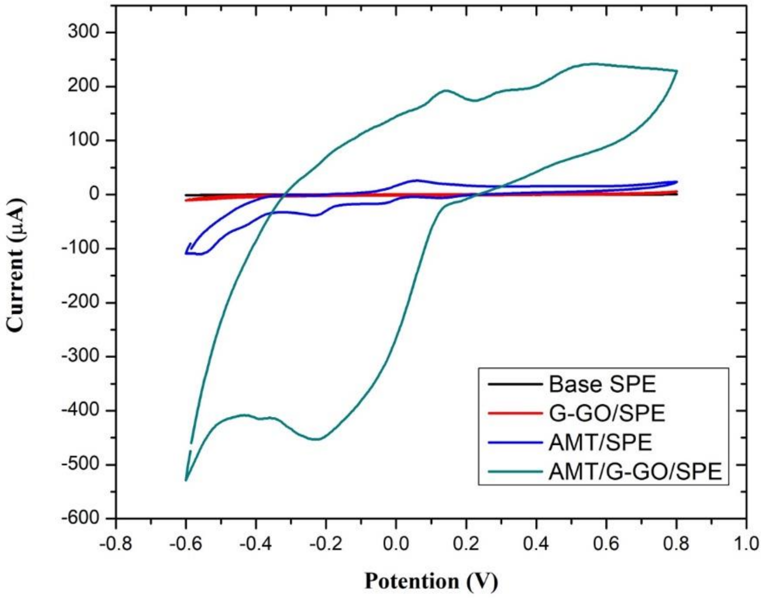

Figure 3. Cyclic voltammograms of different modified electrodes to detect 1 mM test solution of calcium phosphate.

3.4 Effect of scan rate

In order to evaluate the effect of scan rate on the oxidation of phosphate at AMT/G-GO/SPE, linear sweep voltammetry (LSV) was performed using a 1 mM test solution of calcium phosphate.

The scan rate was changed from 20 to 200 mV/s with an interval of 20 mV/s. As shown in Figure 4, the peak reduction current of phosphate increased with the increase of the scan rates. Furthermore, the peak current was linearly proportional to the square root of the scan rate. This relationship explains that the diffusion coefficient could be regarded as 1, meaning that the semi-infinite diffusion of the electroactive substance on the electrode surface was consistent. That is, the test solution could diffuse and reach the electrode surface. The phosphate reaction at the AMT/G-GO/SPE is a diffusion-controlled process. This result is consistent with the results reported in the previous literatures [41, 42]. If the peak current has a linear relationship with the square roots of the scanning rates, it indicats the redox process to be a diffusion controlled electrochemical process.

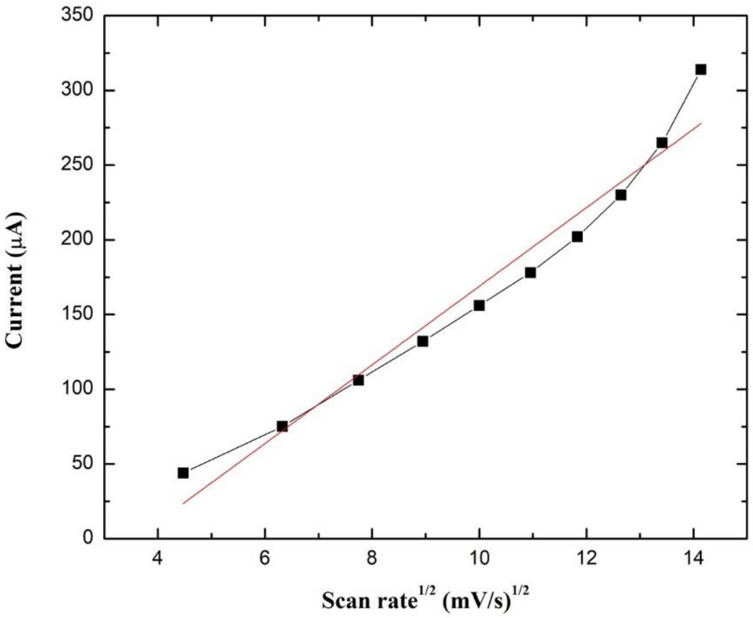

Figure 4. Effect of scan rate under linear sweep voltammetry at various scan rates from 20 to 200 mV/s with an interval of 20 mV/s.

3.5 Measurement of different phosphate levels

Generally speaking, the physiological concentration of phosphate in the human body remains in a stable range of 2.5 – 4.5 mg/dL (i.e. 0.81 – 1.45 mM). Different phosphate concentrations were employed and measured with CV to investigate the applicability of AMT/G-GO/SPE in determining phosphate levels.

The test range was 0.2 to 5 mM. Further, to ensure accurate measurement within the normal physiological value range of the human body, 10 test sets were performed in the range of 0.2 – 2 mM with an interval of 0.2-mM. The experiments were carried out according to the aforementioned procedure using a 200 μL test solution, and three AMT/G-GO/SPE sensors were prepared for each concentration for repetitious experiments.

Figure 5 shows that the absolute value of the peak reduction current was linearly related to the phosphate concentration, described by the regression equation $y = 97.69x + 130.4772$, where y is the current (μA) and x is the phosphate concentration (mM), with the coefficient of determination R^2 = 0.9904. The experimental result reveals that this proposed AMT/G-GO/SPE sensor is suitable for detecting phosphate levels in the physiological concentration range and higher concentration range. The detailed comparison of this work with the previous published electrochemical phosphate sensors is listed in Table 1.

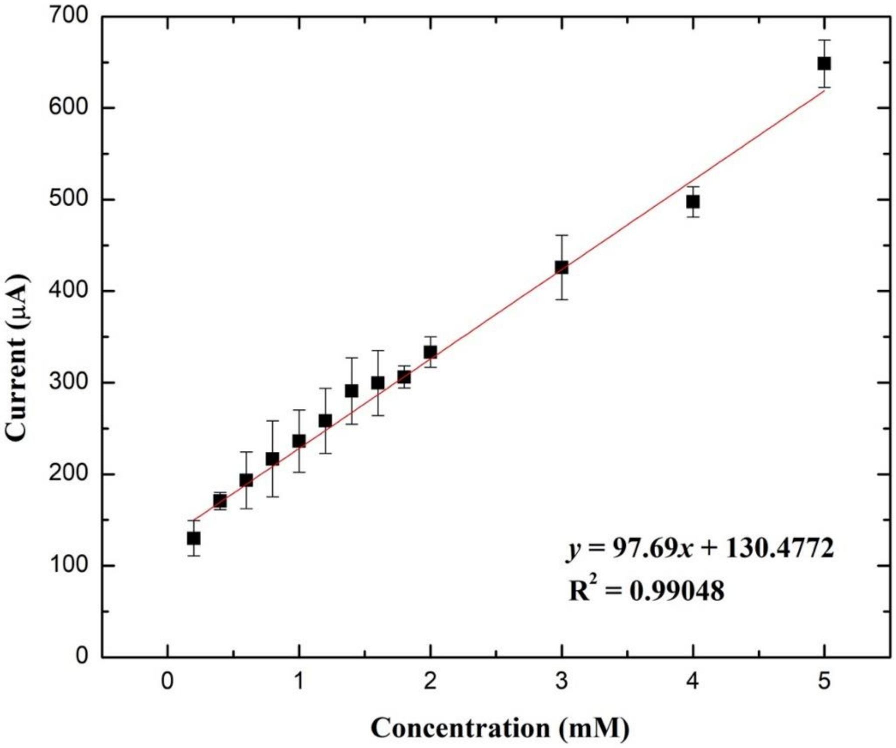

Figure 5. Linear relationship between the absolute value of the peak reduction current and the phosphate concentration from 0.2 to 5 mM.

Table 1. Some existing electrochemical SPE sensors to detect phosphate using molybdate

Working electrode	Electrochem. method	Analyte	Linear range	Ref.
CBNPs/SPE [a]	Amperometry	Water sample	1–80 μM	23
CBNPs/SPE [a]	Amperometry	Water sample	0.5–100 μM	31
Paper-CB-SPE	CV	Water sample	10–300 μM	33
ZrO_2/ZnO/MWCNTs/AMT/SPE [b]	CV	Soil sample	0.037–1.1 μM	39
AHM@PANI/CC/PVDF [c]	CV	Water sample	10–114 μM	40
AMT/G-GO/SPE	CV	Calcium phosphate	0.2–5 mM [d]	This work

[a] Carbon black nanoparticles

[b] Zirconium dioxide/zinc oxide/multiple-wall carbon nanotubes/ammonium molybdate tetrahydrate/SPE

[c] Ammonium heptamolybdate (AHM)/polyaniline (PANI)/coconut shell-derived carbon (CC)/poly(vinylidene fluoride-co-hexafluoropropylene)

[d] To cover the physiological concentration of phosphate in human body

3.6 Anti-interference study

Anti-interference is an essential assay to ensure that AMT/G-GO/SPE has good selectivity in detecting phosphate levels without suffering from the influences generated by the coexisting chemicals in the human body. In the interference experiment, 100 mL of 1 mM calcium phosphate solution was mixed with 10 mM of the target interferent powder and stirred by a rotor for 30 min. Then, 200 μL of the test aqueous solution was extracted by micropipette to cover all electrodes of AMT/G-GO/SPE for cyclic voltammetry. The considered interferents were divided into the interfering substances in urethral calculus and the interfering substances in human blood. The calculus interferents include uric acid (UA) and oxalic acid (OA); the interferents in human blood include ascorbic acid (AA), dopamine (DA), glucose (Glu), calcium ion, copper ion, ferri ion, and nitrite ion.

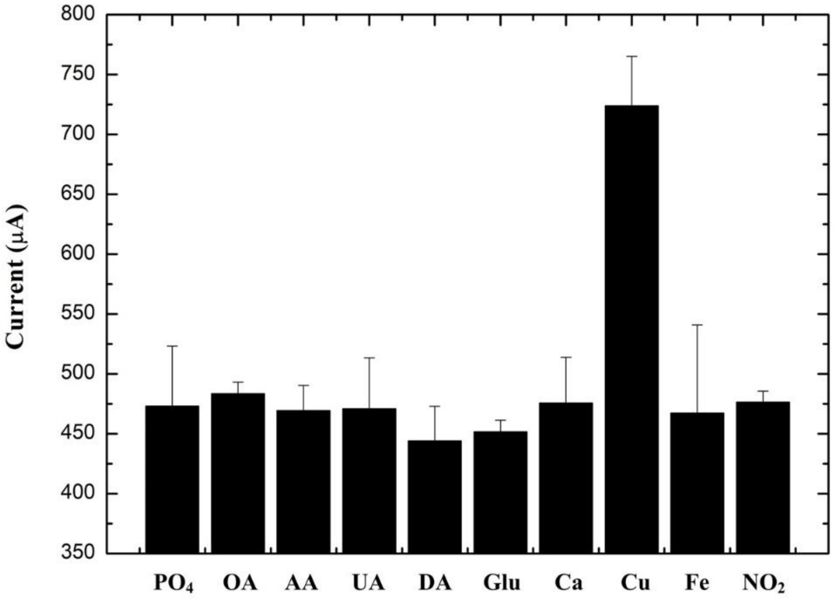

Figure 6. Anti-interference study of 1 mM calcium phosphate solution mixed with 10 mM interfering compounds by CV measurements at -0.2023 V.

Each bar in Figure 6 represents the current measured at -0.2023 V when the phosphate solution was mixed with an aforementioned interferent. The voltage -0.2023 V was the potential at which the phosphomolybdate had a peak reduction current. This bar chart shows the effect of CV measurement of AMT/G-GO/SPE subjected to interferents. No evident signal changes were found for most interfering substances, and the changes in the current signals were within 5% of the original signal without adding interferents. The results reveal that most interference factors did not influence the phosphate detection of AMT/G-GO/SPE. However, the peak current rose significantly when the copper ions were applied. Therefore, copper ion is an interference factor to phosphate detection using AMT/G-GO/SPE. Since copper ion is a metal ion, it enhances the conductivity of the experiment and generates a higher peak current. Even so, AMT/G-GO/SPE exhibits excellent anti-interference performance, which can be used to detect the content of phosphate in urethral calculus or human blood.

4. CONCLUSIONS

Detecting phosphoric acid-derived phosphate is of great significance to environmental and biological systems. In this study, an electrochemical phosphate sensor modified with graphene–graphene oxide nanocomposite and ammonium molybdate was developed to quantitatively determine phosphate levels. This proposed sensor has many advantages, including low consumption of analyte solution, high sensitivity, and good selectivity. Furthermore, the detection range of phosphate covers normal physiological concentrations and higher concentrations without suffering from the interfering substances in urethral calculus and human blood. Therefore, the sensor is suitable for environmental surveillance, human physiological monitoring, and urethral calculus analysis.

ACKNOWLEDGMENT
This work was supported by the National Science and Technology Council (NSTC) of Taiwan, R.O.C. [grant number MOST 110-2221-E-033-024-MY2]

References

1. M. Edén, *Materialia*, 17 (2021) 101107.
2. L. Chen, S. Al-Bayatee, Z. Khurshid, A. Shavandi, P. Brunton and J. Ratnayake, *Materials*, 14 (2021) 4865.
3. G. Kazakova, T. Safronova, D. Golubchikov, O. Shevtsova and J.V. Rau, *Materials*, 14 (2021) 4857.
4. E. Possik, A. Al-Mass, M.-L. Peyot, R. Ahmad, F. Al-Mulla, S.R.M. Madiraju and M. Prentki, *Front. Endocrinol.*, 12 (2021) 706607.
5. J. Yee, D. Rosenbaum, J.W. Jacobs and S.M. Sprague, *Am. J. Nephrol.*, 52 (2021) 522.
6. E. Habas Sr., M. Eledrisi, F. Khan and A.-N. Elzouki, *Cureus*, 13 (2021) e16388.
7. H. Wang, L. Zhang, W. Liao, J. Huang, J. Xu, J. Yang, C. Chen and Z. He, *Clin. Biochem.*, 91 (2021) 9.
8. S. Fukumoto, *Encyclopedia Endocr. Dis*., 4 (2018) 68.
9. M. Pourhassan, M.J. Müller, D. Volkert and R. Wirth, *Eur. J. Clin. Nutr.*, 73 (2019) 634.
10. X.Y. Sun, J.M. Ouyang, F.X. Wang and Y.S. Xie, *J. Nanomater*., 5 (2015) 1.
11. S. Li, V. Iremashvili, S.L. Vernez, K.L. Penniston, R.A. Jhagroo, S.L. Best, S.P. Hedican and S.Y. Nakada, *Can. J. Urol.*, 28 (2021) 10744.
12. R. Flanngian, W.H. Choy, B. Chew and D. Lange, *Nat, Rev. Urol.*, 11 (2014) 333.
13. X. Gao, C. Lu, F. Xie, L. Li, M. Liu, Z. Fang, Z. Wang, S. Ming, H. Dong, R. Shen, Y. Sun, Y. Peng and X. Gao, *World J. Urol.,* 38 (2020) 219.
14. A. Kyaw, K. Maung-U and T. Toe, *Anal. Biochem.*, 145 (1985) 230.
15. W. Liu, Z. Du, Y. Qian and F. Li, *Sens. Actuator B-Chem.*, 176 (2013) 927.
16. Y. Wang, W. Weng, H. Xu, Y. Luo, D. Guo, D. Li and D. Li, *Anal. Chim. Acta*, 1080 (2019) 196.
17. V. Choudhary and L. Philip, *Microchem. J.*, 171 (2021) 106809.
18. K. Ikebukuro, H. Wakamura, I. Karube, I. Kubo, M. Inagawa, T. Sugawara, Y. Arikawa, M. Suzuki and T. Takeuchi, *Biosens. Bioelectron.*, 11 (1996) 959.
19. M. Yaqoob, A. Nabi and P.J. Worsfold, *Anal. Chim. Acta*, 510 (2004) 213.
20. Y. Ma, Y. Zhang, X. Li, P. Yang, J.-Y. Yue, Y. Jiang and B. Tang, *Anal. Chem.*, 92 (2020) 3722.
21. Y. Udnana, I.D. McKelvie, M.R. Grace, J. Jakmunee and K. Grudpan, *Talanta*, 66 (2005) 461.

22. L. Glibert, A.T.A. Jenkins, S. Browning and J.P. Hart, *Sens. Actuators B-Chem.*, 160 (2011) 1322.
23. D. Talarico, S. Cinti, F. Arduini, A. Amine, D. Moscone and G. Palleschi, *Environ. Sci. Technol.*, 49 (2015) 7934.
24. C. Barus, I. Romanytsia, N. Striebig and V. Garçon, *Talanta*, 160 (2016) 417.
25. X. Zhou, Z. He, Q. Lian, Z. Li, H. Jiang and X. Lu, *Sens. Actuators B-Chem.*, 193 (2014) 198.
26. F. Ahour and M.K. Ahsani, *Biosens. Bioelectron.*, 86 (2016) 764.
27. A. Gevaerda, S.F. Blaskieviczb, A.J.G. Zarbinc, E.S. Orthb, M.F. Bergaminia and L.H. Marcolino-Junior, *Biosens. Bioelectron.*, 112 (2018) 108.
28. S. Fatma, B.B. Prasad, S. Jaiswal, R. Singh and K. Singh, *Biosens. Bioelectron.*, 135 (2019) 36.
29. Y. Xing, C. Zhang, X. Chen, H. Zhao and Z. Guo, *Biomed. Anal.*, 206 (2021) 114389.
30. V.T. Le, Y. Vasseghian, E.-N. Dragoi, M. Moradi and A.M. Khaneghah, *Food Chem. Toxicol.*, 148 (2021) 111931.
31. D. Talarico, F. Arduini, A. Amine, D. Moscone and G. Palleschi, *Talanta*, 141 (2015) 267.
32. M.B. Arvas, O. Groduk, M. Gencten and Y. Sahin, *Anal. Methods*, 11 (2016) 78.
33. S. Cinti, D. Talarico, G. Palleschi, D. Moscone and F. Arduini, *Anal. Chim. Acta*, 919 (2016) 78.
34. M. Khenfouch, U. Buttner, M Baïtoul and M. Maaza, *Graphene*, 3 (2014) 7.
35. E. Jaafar, M. Kashif, S.K. Sahari and Z. Ngaini, *Mater. Sci. Forum*, 917 (2018) 112.
36. Z. Zhang, H.C. Schniepp and D.H. Adamson, *Carbon*, 154 (2019) 510.
37. E. Aliyev, V. Filiz, M.M. Khan, Y.J. Lee, C. Abetz and V. Abetz, *Nanomaterials*, 9 (2019) 1180.
38. J. Phiri, L.-S. Johansson, P. Gane and T. Maloney, *Compos. Pt. B-Eng.*, 147 (2018) 104.
39. Y. Lu, Q. Lan, C. Zhang, B. Liu, X. Wang, X. Xu and X. Liang, *Environ. Sci. Technol.*, 55 (2021) 13093.
40. D.R. Kumar, G. Dhakal, V.Q. Nguyen, J. Lee, Y.R. Lee and J.-J. Shim, *Microchem. J.*, 170 (2021) 106639.
41. Q. Yan, N. Zhi, L. Yang, G. Xu, Q. Feng, Q. Zhang and S. Sun, *Sci. Rep.*, 10 (2020) 10607.
42. J.A. Buledi, S. Ameen, S.A. Memon, A. Fatima, A.R. Solangi, A. Mallah, F. Karimi, S. Malakmohammadi, S. Agarwal and V.K. Gupta, *Open Chem.*, 19 (2021) 481.